

## X-ray-absorption studies of krypton precipitates in solid matrices

Zhengquan Tan,\* J. I. Budnick, D. M. Pease, and F. Namavar†

*Department of Physics and Institute of Materials Science, University of Connecticut, Storrs, Connecticut 06269-3046*

(Received 14 May 1990; revised manuscript received 3 August 1990)

Krypton  $K$ -edge x-ray-absorption spectra have been measured at 300 and 80 K on samples of krypton-implanted Al and Nb foils, graphite, and Grafoil. The near-edge spectra (XANES) at both 300 and 80 K exhibit a white line. Comparisons with the XANES data of bulk solid krypton and spectra amongst different host materials suggest that the krypton in all the implanted hosts precipitates into bubbles at high dosages. The bubbles in Nb hosts are probably all in the solid phase even at 300 K. For Al, graphite, and Grafoil, the bubbles appear to exist in both solid and nonsolid form. The Kr-Kr nearest-neighbor distance in the solid Kr precipitates is estimated from XANES data using an empirical relation deduced from data on bulk solid krypton under high pressure. High pressure within the Kr precipitates is revealed from the smallness of the lattice parameter and the lattice expansion at low temperature. Extended x-ray-absorption fine structure is observed only on a postimplantation thermally annealed Al sample and an as-implanted Nb sample.

### I. INTRODUCTION

Rare-gas atoms in solid matrices produced by ion implantation or nuclear reactions are insoluble and often precipitate into microclusters, commonly referred to as bubbles. The cluster state and formation mechanism have received considerable attention for both fundamental and practical reasons. It has been found that the bubbles of light rare gases<sup>1-3</sup> are in the gas or liquid form while the heavy ones (Kr and Xe) (Refs. 3-11) are present in the solid phase. In particular, Kr and Xe form face-centered-cubic (fcc) crystallites in fcc (Refs. 4, 6, 7, and 11) and body-centered-cubic (Ref. 8) (bcc) hosts at room temperature for implant doses of the order of  $10^{16}$ - $10^{17}$  ions/cm<sup>2</sup>. In hosts of hexagonal-close-packed (hcp) structure, hcp bubbles were found,<sup>5,11</sup> but fcc bubbles may also be present. The lattice parameter of the solid bubbles is significantly less than the bulk value under ambient pressure. This has been attributed to high pressures, of the order of GPa within the bubbles. These high pressures were also inferred from optical-absorption and electron-energy-loss spectroscopy experiments for He bubbles<sup>1</sup> and Ne, Ar, and Xe bubbles in aluminum hosts.<sup>3</sup> The bubble size and bubble pressure depend strongly on the nature of the host materials and the implant doses. The understanding of the bubble formation process and the rich phenomena observed is still limited at the present time. In an effort to study the krypton local environment in the implanted matrices, we have carried out x-ray-absorption measurements at the krypton  $K$  edge on samples of aluminum, niobium, graphite, and Grafoil implanted to doses up to  $5 \times 10^{17}$  Kr/cm<sup>2</sup>. The absorption spectra exhibit structure in the near-edge region (XANES), but only in two cases showed extended fine structure (EXAFS). We will discuss mostly the XANES data.

### II. EXPERIMENT

The ion implantation was carried out on a medium-energy implanter in a vacuum of  $10^{-6}$  Torr using a scan-

ning beam of 150-160-keV Kr<sup>+</sup> at current rates less than  $10 \mu\text{A}/\text{cm}^2$ . The target was generally kept at room temperature except that for Nb the target temperature was 100°C. Target materials are polycrystalline pure metal foils, graphite, and Grafoil. The Grafoil has the same crystal structure as graphite but a much shorter coherence length among the crystallites and is softer. In addition, the crystallites are preferentially oriented with the basal planes parallel to the macroscopic Grafoil surface.<sup>12</sup> The Kr concentration profile in the implanted hosts was measured by Rutherford backscattering spectrometry (RBS) using a 1.5-MeV He<sup>+</sup> beam. X-ray-absorption measurements were made at the National Synchrotron Light Source (NSLS) on beam line X-11A using a Si(111) double-crystal monochromator. The Kr  $K$ -edge (14 322 eV) absorption spectra of implanted samples were obtained at temperatures of 300 and 80 K by monitoring the incident and fluorescence flux intensities. Spectra were also acquired for Kr gas and for solid Kr by condensing Kr gas at near liquid-nitrogen temperatures. Both transmission and fluorescence measurements were made on condensed Kr of various thickness. Variations among our spectra representative of those reported<sup>13-15</sup> were observed. Our transmission spectra on samples with absorption thickness ( $\mu x$ ) of about 1.0 and the fluorescence spectra on samples with  $\mu x \cong 0.1$  agree with each other, and both agree with those reported by Soules *et al.*<sup>13</sup> and Kutzler *et al.*<sup>14</sup> Therefore, we will use this spectrum for solid krypton. The energy was calibrated by simultaneously measuring the spectrum of Kr gas in a reference channel.

### III. RESULTS AND DISCUSSION

The concentration depth profile of Kr in Al, graphite, and Grafoil was measured by RBS. Four Al samples with doses of 0.5, 1.0, 1.6, and  $2.0 \times 10^{17}$  Kr/cm<sup>2</sup> all show a Kr concentration peaked in the range 900-1000 Å. The Kr peak concentration already reaches 7% at a dose of  $5 \times 10^{16}$  Kr/cm<sup>2</sup>, increases to 9% at  $1.0 \times 10^{17}$  Kr/cm<sup>2</sup>,

and drops to 8% with a broader distribution at  $2 \times 10^{17}$  Kr/cm<sup>2</sup>. For graphite samples, the peak concentration is at 700 Å with a similar dose dependence as in Al samples. The highest concentration of about 8% is achieved at a dose of  $1 \times 10^{17}$  Kr/cm<sup>2</sup>. The Kr concentration in the Grafoil is one-fifth to one-fourth of that in graphite at similar doses. Implantation with varying beam energies (150, 100, and 55 keV) was able to increase the Kr retention slightly. The Kr concentration in Nb hosts has not been determined precisely since the atomic mass of Kr is close to that of Nb. However, the amount of total krypton in Nb samples is comparable to that in similar Al samples as estimated from the step sizes at the Kr x-ray-absorption edge.

In an x-ray-absorption event, a core-level electron with well-defined orbital symmetry is excited to a final state that is selected by the dipole rule. The XANES data (viz., the features near the absorption edge) generally reflect the coordination geometry, coordination number, and the nature of chemical bonding with neighbor atoms. However, a unified theoretical interpretation of the XANES spectrum, especially the edge structure, is presently not available. Useful information is often extracted by comparison with reference spectra measured on known materials. Strong peaks, often termed "white lines," can occur near the absorption edge due to atomic-like bound states, molecular orbitals, or unoccupied density of states in a condensed system. In the present case of krypton *K*-edge absorption, molecular orbitals are ruled out since Kr interacts rather weakly with other atoms. Transitions to the Rydberg series (which give rise to white lines in the *K* absorption spectra of atomic neon and argon<sup>16</sup>) are wiped out by the strong core-hole lifetime broadening. Thus, the absorption spectrum of atomic krypton is essentially structureless (Fig. 1). In solid krypton, a white line is observed at the absorption edge<sup>13-15,17</sup> (Fig. 1). In a multiple-scattering calculation using a Kr<sub>13</sub> cluster (absorber plus the twelve nearest neighbors in the fcc lattice), Kutzler *et al.*<sup>14</sup> were able to qualitatively reproduce the first two peaks observed. In this picture, the white line is a result of backscattering from the Kr near neighbors.

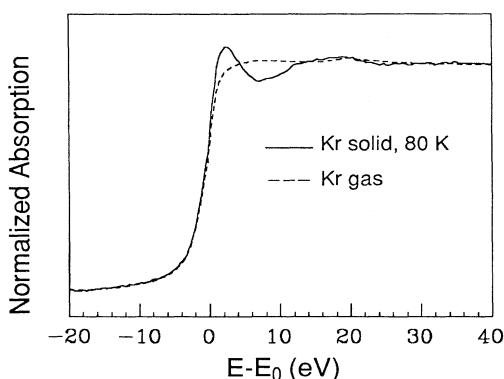


FIG. 1. Kr *K*-edge XANES spectra for krypton gas and solid at 80 K.

The XANES spectra presented here have been normalized to the step size after the preedge background subtraction. The energy origin ( $E_0$ ) was chosen at the inflection point (the first maximum in the derivative). Figure 1 presents the XANES data for the gas phase and the solid phase (80 K) of krypton. The gas spectrum is atomic and shows little structure. The solid krypton spectrum exhibits a white line above the edge followed by a few oscillations representing the backscattering from Kr neighbors. The oscillations are damped out quickly at higher energies due to large thermal vibrations. To an estimated uncertainty of 1 eV, we observe no energy shift between the absorption edges of Kr gas and Kr solid. Shifts of 4 eV (Ref. 13) and 1 eV (Ref. 14) to higher energies for the solid Kr have been previously reported.

Figures 2(a)–2(c) present Kr XANES spectra for Kr in Nb, Al, and graphite and Grafoil hosts. All the implanted samples show a white line followed by a weak peak in the absorption spectra even at 300 K. The white line at 80 K is enhanced in the case of Al and Grafoil hosts. The Kr XANES and the white line enhancement at 80 K for the graphite samples are similar to those for the Grafoil, thus the term carbon will also be used for one or both of the graphite and Grafoil hosts in our discussion. The observed XANES could be caused by host atoms and/or krypton atoms. The backscattering power for carbon, Al, and Nb atoms is generally different. If scattering from the host atoms is significant, the XANES spectra, in particular the white line, should vary for the three different hosts. At 80 K, the white line intensity and line shape as shown in Fig. 3 for Kr in graphite, Al, and Nb hosts are surprisingly similar. This suggests that the XANES spectra in the implanted samples are all due to krypton neighbors rather than the host atoms. In the literature, we found only the Kr-C, other than Kr-Kr, XANES behavior. This was observed in a study<sup>18</sup> of krypton on a Grafoil surface in which the Kr-C XANES was isolated. In the Kr-C XANES, the amplitude of the second peak is comparable to the first one (white line) at 100 K, and becomes stronger at 20 K due to the reduction of the large thermal vibration ( $\Delta\sigma^2=0.051 \text{ \AA}^2$ ). For the Kr-Kr XANES at 80 K (Fig. 1) and 300 K (Ref. 17) the first peak is always stronger than the second. In view of this characteristic, the observed XANES spectra point to backscattering from Kr near neighbors. Therefore our observed XANES spectra indicate that the majority of Kr in the implanted matrices is in the form of krypton precipitates. We note that this is a nontrivial result, since the x-ray absorption probes all Kr atoms in the host, while imaging and diffraction techniques detect the solid bubbles but cannot determine the amount that is not in the bubble form. The krypton precipitation is consistent with the low solubility of a rare gas in solid matrices.

For Kr in Nb hosts [Fig. 2(a)] the white line at 300 K is nearly as strong as that at 80 K. The white line is due to strong pair correlations that could exist in either liquid or solid phases. In order to distinguish these two possibilities, it would be ideal to compare the spectrum of Kr precipitates with that of a liquid krypton. The existence of strong pair correlations at 300 K implies that all the bubbles must be in the solid phase at 80 K, since krypton gas

(in which there is no pair correlation) solidifies at 116 K under ambient temperature. Similarly, the Kr bubbles in Al and carbon hosts are also in the solid phase at 80 K. If we examine the XANES spectra at 300 K more closely, further information about the nature of the Kr bubbles can be obtained. The Kr-Kr nearest distance estimated

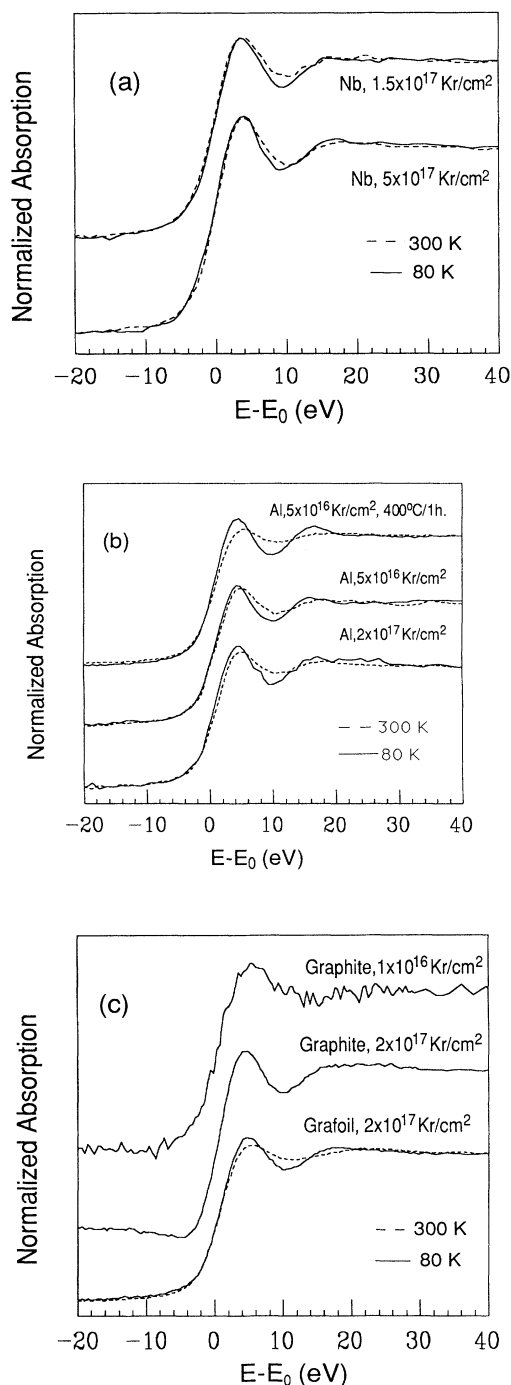


FIG. 2. Kr *K*-edge XANES spectra at 300 K (dashed line) and 80 K (solid line) for krypton implanted in (a) Nb foils, (b) Al foils, and (c) graphite and Grafoil.

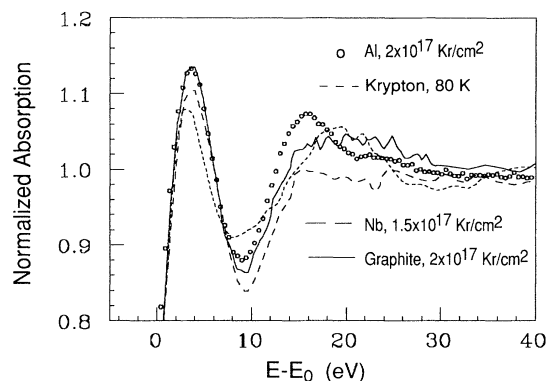


FIG. 3. Normalized Kr XANES at 80 K, comparing the white line for the implanted samples and bulk solid krypton at 80 K.

from the position of the peak following the white line (see below) suggests that at 300 K the bubbles in the Nb hosts are also in the solid phase. The slight broadening of the white line at 300 K is probably due to the higher pressure in the bubbles (see below). There is no significant variation between the XANES spectra of Nb samples implanted to above  $1 \times 10^{17}$  Kr/cm<sup>2</sup>, suggesting that the Kr bubbles are of similar nature at high dosages.

An enhancement of the white line at 80 K is observed for the Kr in Al and carbon hosts. The Kr precipitates are expected to be in the solid phase at 80 K. The white line enhancement at 80 K is quite unusual if all Kr bubbles are also in the solid phase at 300 K, as discussed in our previous report<sup>19</sup> where some possible causes for the white line enhancement were surveyed. In addition, we note that a reduced thermal vibration will enhance the second peak more than the first peak; the Kr-C XANES of Bouldin and Stern<sup>18</sup> being a specific example. The white line enhancement cannot be attributed to thermal vibrations for several reasons. First, the white line is more strongly enhanced than the second peak. Second, the thermal vibration effect is expected to be qualitatively similar for Kr bubbles in Al and Nb hosts, while enhancement in the Nb hosts is much smaller. Third, reduction of the thermal vibrations at higher pressure does not give an observable white line enhancement for the bulk solid krypton.<sup>17</sup> We interpret the observed white line enhancement as being due to the condensation at 80 K of some liquid or gaseous bubbles in Al and carbon hosts at 300 K. At 300 K these nonsolid bubbles contribute to the absorption edge but contribute weakly to the white line, thus resulting in a weaker averaged white line. Evidence for nonsolid bubbles was also inferred<sup>7</sup> from the diffuse diffraction pattern in Al hosts for doses above  $2 \times 10^{16}$  Kr/cm<sup>2</sup>.

The crystal structure of the krypton bubbles can be influenced by the lattice structure of the host. Kr bubbles in fcc and bcc hosts are known to assume the fcc structure.<sup>4,6-8,11</sup> Thus the solid bubbles in the fcc Al and bcc Nb hosts are expected to be of fcc structure. The graphite is hexagonal and is highly two-dimensional (2D). The

Grafoil also has a graphitic structure, but the crystallites are aligned with the basal planes parallel to the macroscopic surface. At high doses ( $\geq 1 \times 10^{17}$  Kr/cm<sup>2</sup>), we observe no significant difference between the XANES spectra for Kr in graphite and in Grafoil, even though the retention of Kr in the latter is much lower. Typical bubble sizes observed in other hosts are greater than 20 Å (Refs. 5, 7, and 10), much larger than the spacing between adjacent basal planes in the graphite structure. It is very likely that the Kr bubbles in samples implanted to high dosages are quite large and their final form is not affected by the preferred orientation of the host crystallites in the Grafoil. At  $1 \times 10^{16}$  Kr/cm<sup>2</sup>, the white line is much broader than at  $2 \times 10^{17}$  Kr/cm<sup>2</sup>. At this dose, some Kr bubbles may also exist and the bubble sizes are likely to be smaller than those at higher doses. The higher pressure in the smaller bubbles will contribute to the white line broadening. Another source for the different XANES spectra observed at  $1 \times 10^{16}$  Kr/cm<sup>2</sup> may be the existence of krypton atoms that are not clustered in the same way as those at high doses. 2D-like Kr clusters or even intercalation may exist due to the 2D nature of the graphite structure. Polarized XANES measurements on krypton implanted in Grafoil may help to detect possible 2D-like Kr clusters. It will also be interesting to learn about the structure of the bubbles at high doses.

Figure 3 shows the Kr XANES spectra at 80 K for Al, Nb, and graphite hosts all implanted to about  $2 \times 10^{17}$  Kr/cm<sup>2</sup>. The solid krypton spectrum is included for comparison. The details of the XANES spectra depend on the nature of the host material. However, the white line peaks from Kr in C, Al, and Nb hosts are similar to each other and are slightly stronger than that of bulk solid krypton. The slightly stronger white line in the implanted samples may originate from a denser packing of Kr atoms in the bubbles, which are under high pressures,

as will become clear later. In all cases, the white line of the implanted samples is broader than that of the bulk krypton. For the bulk solid krypton under high pressure,<sup>17</sup> the white line becomes progressively broadened as the pressure increases even though the thermal vibration is reduced. The broader white line for the implanted samples may also be due to the high pressure in the krypton bubbles. Another source for the broadening could be an inhomogeneous environment in the implanted material.

The second XANES peak at 80 K shifts to lower energies as compared to 300 K for Kr implanted in Al, Nb, and carbon hosts. The energy of the second peak ( $E$ ) measured relative to the threshold is listed in Table I. The shift to lower energies indicates a lattice expansion in the Kr bubbles. In general, a decrease in the XANES and EXAFS peak energy is indicative of an increase in the bond length; and, in particular, this relation is found to hold for bulk krypton.<sup>17</sup> A lattice parameter increase with decreasing temperature is also observed by Andersen *et al.*<sup>6</sup> for krypton bubbles in Al hosts. It is known that bulk solid krypton contracts with decreasing temperature under constant pressure.<sup>20</sup> However, the krypton bubbles in the solid matrices are in a quite different situation. The bubbles are confined to a cavity within the solid and are under high pressure. The pressure within the bubble is largely determined by  $2\gamma^*/r$ , where  $\gamma^*$  is the effective surface tension of the cavity (host material) and  $r$  is the radius of the bubble (assuming a spherical shape).  $\gamma^*$  is expected to be nearly temperature independent for temperatures below 300 K. As the temperature decreases, the pressure within the Kr bubbles tends to decrease. The decrease in the pressure can be achieved by an increase in the radius  $r$ , i.e., by expansion of the bubble. The pressure within the bubble is so high that the expansion is not suppressed by the host matrix. The krypton lattice expansion at low temperature is due to

TABLE I. The energy ( $E$ , from the first inflection point) of the second Kr  $K$ -edge XANES peak, average Kr-Kr nearest-neighbor distance ( $R_1$ ), and the pressure ( $P$ ) of krypton solid bubbles in implanted materials. The  $R_1$  values are deduced from  $E$  and an empirical relation  $E$  (eV) =  $54.6 - 10.6R_1$  (Å). The pressure is obtained from the reported  $P$  versus lattice parameter relation for bulk fcc solid krypton at room temperature [Polian *et al.* (Ref. 17)]. The estimated uncertainties in  $E$  and  $R_1$  are 1.5 eV and 0.2 Å, respectively.

Samples	$E$ (eV)	$T=300$ K		$T=80$ K	
		$R_1$ (Å)	$P$ (GPa)	$E$ (eV)	$R_1$ (Å)
KrAl-C (30 at. % Kr) <sup>a</sup>	16.2	3.6	3.4		
KrAl-F (10 at. % Kr)	15.5	3.7	2.8		
KrAl ( $2 \times 10^{17}$ )	18.9	3.4	9.4	16.0	3.6
KrAl ( $5 \times 10^{16}$ )	19.2	3.4	10	14.8	3.8
KrAl ( $5 \times 10^{16}$ , 400°C/1 h)	17.5	3.5	5.7	15.3	3.7
KrNb ( $1.5 \times 10^{17}$ )	19.2	3.4	10	16.5	3.6
KrNb ( $5 \times 10^{17}$ )	19.2	3.4	10	16.5	3.6
Grafoil ( $2 \times 10^{17}$ ) <sup>b</sup>	21.7	3.1		15.7	3.7
Graphite ( $1 \times 10^{17}$ , 300°C/5 h)	20.0	3.3		18.1	3.4
Graphite ( $2 \times 10^{17}$ )	21.7	3.1		19.6	3.3

<sup>a</sup>Implanted with multiple energies to achieve a uniform nominal atomic concentration 30 at. % Kr.

<sup>b</sup>Total dose, implanted with 1.0, 0.64, and  $0.4 \times 10^{17}$  Kr/cm<sup>2</sup> at energies of 150, 100, and 55 keV, respectively.

the decrease of the bubble pressure as the temperature is lowered.

Polian *et al.*<sup>17</sup> have reported a correlation between the energy ( $E$ , relative to the threshold) of the second XANES peak and the lattice parameter ( $a$ ) of fcc bulk krypton at 300 K under high pressure. Using their data for  $E$  versus pressure ( $P$ ) and  $a$  versus  $P$ , we have plotted the  $E$  versus the Kr-Kr nearest-neighbor distance ( $R_1$ ) in Fig. 4. The data points seem to fall on a straight line, and a linear least-squares fit yields  $E$  (eV) =  $54.6 - 10.6R_1$  (Å). This empirical relation is then applied to the krypton bubbles (only the solid ones) in Al and Nb at 300 and 80 K under the assumption that the krypton bubbles have the fcc structure and behave similarly to the bulk krypton under high pressure. The uncertainty in such an estimate is inevitably large, since the value of  $R_1$  is sensitive to the value of  $E$ , and the accuracy in determining  $E$  is limited when the XANES peak is broad. Another source of error is that the energy origin determined in our work may differ slightly from that in Ref. 17. Apparently, use of the  $E$  versus  $R_1$  relation on our solid krypton at 80 K gives a too-small  $R_1$  value. The  $R_1$  value for Kr bubbles is expected to be an underestimate and consequently the bubble pressure is overestimated. Nevertheless, a relative comparison of these estimated parameters between 300 and 80 K should be meaningful.

The Kr-Kr nearest-neighbor distances obtained from the relation  $E$  (eV) =  $54.6 - 10.6R_1$  (Å) are listed in Table I for Al and Nb samples. The associated bubble pressure is estimated from the  $a$  versus  $P$  data of Ref. 17. The Kr-Kr distances are all smaller than the 3.99 Å value of fcc krypton at 4.2 K under ambient pressure. The bubble pressure is in excess of the melting pressure 0.85 GPa for Kr at 300 K,<sup>21</sup> in accordance with the existence of solid bubbles. Our estimated lattice parameter values for the

Kr bubbles in Al hosts are in qualitative agreement with values reported by Andersen *et al.*<sup>6</sup> and Birtcher and Jäger.<sup>7</sup>

The Kr bubbles in the graphite and Grafoil hosts may not assume a fcc structure. To estimate the Kr-Kr nearest-neighbor distance, an additional assumption has to be made, i.e., that the second XANES peak is due to the nearest Kr neighbor. This assumption is supported by the calculation of Kutzler *et al.* for bulk solid krypton, which predicted that the Kr nearest neighbor gives rise to the first and the second XANES peaks. Using  $E = 54.6 - 10.6R_1$ ,  $R_1$  is estimated for Kr bubbles in the graphite and Grafoil hosts as listed in Table I. These Kr-Kr distances are smaller than those in Nb and Al hosts, probably suggesting a different crystal structure for bubbles in the graphite and Grafoil hosts. The pressure within the bubbles cannot be estimated since the  $a$  versus  $P$  relation from Polian *et al.* is only for the fcc lattice.

EXAFS oscillations were observed only on two samples, the  $5 \times 10^{16}$  Kr/cm<sup>2</sup> Al sample annealed at 400 °C (sample *A*) and the as-implanted  $1.5 \times 10^{17}$  Kr/cm<sup>2</sup> Nb sample (sample *B*). In a recent x-ray-absorption study of Xe implanted in silicon, Xe EXAFS oscillations were detected only in thermally annealed samples.<sup>22</sup> The EXAFS spectrum and its Fourier transform (inset) of sample *A* are shown in Fig. 5. The overall Fourier-transform spectrum is consistent with what is expected from a fcc structure. The nearest Kr-Kr distance in samples *A* and *B* are determined from the peak position in the Fourier transform plus a correction for the Kr-Kr EXAFS phase shift using theoretically calculated phases.<sup>23</sup> They are 3.66 Å for sample *A* and 3.76 Å for sample *B*. These values are a slight underestimate of the actual value since the effect of relatively large thermal disorder was not taken into account. The Kr-Kr distance determined by EXAFS is consistently greater than those at 300 K deduced from XANES, in support of the lattice expansion at low temperature.

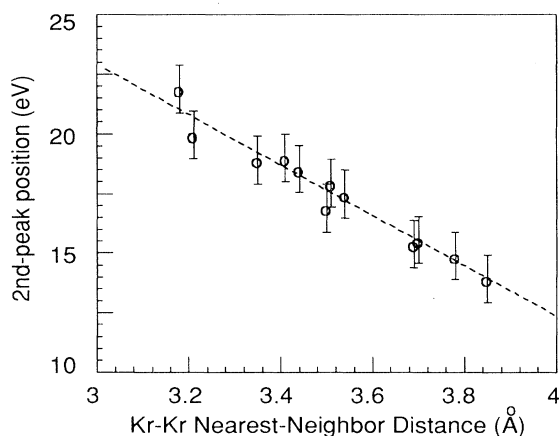


FIG. 4. The energy of the second Kr XANES peak ( $E$ , with respect to the threshold) vs the Kr-Kr nearest-neighbor distance ( $R_1$ ) determined by x-ray diffraction for bulk solid krypton under high pressure at room temperature. Data are taken from Polian *et al.* (Ref. 17). The line is a linear least-squares fit:  $E$  (eV) =  $54.6 - 10.6R_1$  (Å).

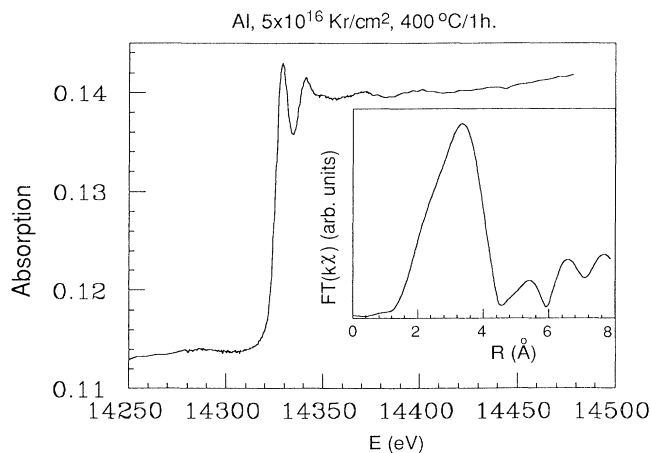


FIG. 5. Kr  $K$ -edge x-ray-absorption spectra for the thermally annealed (400 °C/1 h)  $5 \times 10^{16}$  Kr/cm<sup>2</sup> Al sample. The inset shows the Fourier-transform magnitude of its  $k^{-1}$ -weighted EXAFS function.

#### IV. SUMMARY AND CONCLUSION

The x-ray absorption measures the total contribution of all Kr atoms in the implanted matrix. At 300 K, the white line intensity of Kr in Nb hosts is almost as strong as at 80 K. Therefore, the Kr atoms in Nb hosts are probably all in the solid phase even at 300 K. For Al and carbon hosts, some Kr bubbles are in the solid phase, but nonsolid phases also exist at 300 K. The fact that the lattice parameters are all smaller than that of bulk solid Kr under ambient pressure and the fact that the lattice expands as the temperature is lowered from 300 to 80 K argue for a high pressure in the solid Kr precipitates. The pressure deduced from the lattice parameter is about 10 GPa at 300 K for Kr bubbles in Nb and Al hosts. The state of the precipitates depends on the implant dose for a given host, and depends on the nature of the host for similar dosages. This is demonstrated by the variations

of Kr XANES spectra when these factors are varied. Even when the solid Kr precipitates are under high pressure, the thermal vibrations appear to be large enough to smear out the EXAFS oscillations. The small size of the precipitates may also reduce the EXAFS amplitude significantly.

#### ACKNOWLEDGMENTS

One of us (Z.T.) is pleased to thank Dale Brewe for constructive discussions. We acknowledge the support of the U.S. Department of Energy, Division of Materials Sciences, under Contract No. DE-AS05-80-ER10742 for its role in the development and operation of Beam Line X-11 at the National Synchrotron Light Source (NSLS). The NSLS is supported by the Department of Energy, Division of Materials Sciences and Division of Chemical Sciences under Contract No. DE-AC02-76CH00016.

\*Present address: Brookhaven National Laboratory, Building 480, Upton, NY 11973.

†Now at SPIRE Corporation, Patriots Park, Bedford, MA 01730.

<sup>1</sup>J. C. Rife, S. E. Donnelly, A. A. Lucas, J. M. Gilles, and J. J. Ritsko, *Phys. Rev. Lett.* **46**, 1220 (1981).

<sup>2</sup>R. Manzke, W. Jäger, H. Trinkaus, D. Greclius, R. Zeller, and J. Fink, *Solid State Commun.* **44**, 481 (1982).

<sup>3</sup>A. Vom Felde, J. Fink, Th. Müller-Heinzling, J. Pflüger, B. Scheerer, G. Linker, and D. Kaletta, *Phys. Rev. Lett.* **53**, 922 (1984).

<sup>4</sup>J. H. Evans and D. J. Mazey, *J. Phys. F* **15**, L1 (1985).

<sup>5</sup>J. H. Evans and D. J. Mazey, *J. Nucl. Mater.* **138**, 176 (1986).

<sup>6</sup>H. H. Andersen, J. Bohr, A. Johansen, E. Johnson, L. Sarholt-Kristensen, and V. Sarganov, *Phys. Rev. Lett.* **59**, 1589 (1987).

<sup>7</sup>R. C. Birtcher and Jäger, *Nucl. Instrum. Methods B* **15**, 435 (1986).

<sup>8</sup>J. H. Evans and D. J. Mazey, *Scr. Metall.* **19**, 621 (1985).

<sup>9</sup>G. L. Zhang and L. Niesen (unpublished).

<sup>10</sup>S. E. Donnelley and C. J. Rossouw, *Science* **230**, 1272 (1985).

<sup>11</sup>C. Templier, H. Garem, and J. P. Riviere, *Philos. Mag. (London)* **53**, 667 (1986).

<sup>12</sup>J. K. Kjems, L. Passell, H. Taub, J. G. Dash, and A. D.

Novco, *Phys. Rev. B* **13**, 1446 (1976).

<sup>13</sup>J. A. Soules and C. H. Shaw, *Phys. Rev.* **113**, 470 (1959).

<sup>14</sup>F. W. Kutzler, D. E. Ellis, T. I. Morrison, G. K. Shenoy, P. J. Viccaro, P. A. Montano, E. H. Appelman, L. Stein, M. J. Pellin, and D. M. Gruen, *Solid State Commun.* **46**, 803 (1983).

<sup>15</sup>C. A. Guryan, K. B. Lee, P. W. Stephens, A. I. Goldman, J. Z. Larese, P. A. Heiney, and E. Fontes, *Phys. Rev. B* **37**, 3461 (1988).

<sup>16</sup>For example, see F. C. Brown, in *Synchrotron Radiation Research*, edited by H. Winick and S. Doniach (Plenum, New York, 1980), Chap. 4.

<sup>17</sup>A. Polian, J. P. Itie, E. Dartyge, A. Fontaine, and G. Tourillon, *Phys. Rev. B* **39**, 3369 (1989).

<sup>18</sup>C. E. Bouldin and E. A. Stern, *Phys. Rev. B* **25**, 3462 (1982).

<sup>19</sup>J. I. Budnick, D. M. Pease, M. H. Choi, Z. Tan, G. H. Hayes, F. Namavar, and H. C. Hayden, *J. Phys. (Paris) Colloq.* **47**, C8-1053 (1986).

<sup>20</sup>R. K. Crawford, in *Rare Gas Solids*, edited by M. L. Klein and J. A. Venables (Academic, New York, 1977), Vol. II, p. 777.

<sup>21</sup>Reference 20, p. 694.

<sup>22</sup>G. Faraci, A. R. Pennisi, A. Terrasi, and S. Mobilio, *Phys. Rev. B* **38**, 13 468 (1988).

<sup>23</sup>B. K. Teo and P. A. Lee, *J. Am. Chem. Soc.* **101**, 2815 (1979).